Received: 3 January 2022 | Revised: 5 January 2023 | Accepted: 9 January 2023

DOI: 10.1002/rra.4110

RESEARCH ARTICLE

WILEY

The effect of a local mesh refinement on hydraulic modelling of river meanders

Eray Bilgili[1] | Anouk Bomers[1] | G. Jan-Willem van Lente[2] | Fredrik Huthoff[2] | Suzanne J. M. H. Hulscher[1]

[1]Department of Water Engineering and Management, University of Twente, Enschede, the Netherlands

[2]HKV lijn in water, Lelystad, the Netherlands

Correspondence
Anouk Bomers, University of Twente, P.O Box 217, Enschede, the Netherlands.
Email: a.bomers@utwente.nl

Funding information
Netherlands Organisation for Scientific Research, Grant/Award Number: 14506; Ministry of Economic Affairs and Climate Policy

Abstract

Large-scale river models are generally discretized by relatively large mesh cells resulting in bathymetry discretization errors and numerical effects. These hydraulic models are generally calibrated by altering the bed roughness to compensate for these errors and effects. Consequently, the calibrated roughness values are mesh-dependent while generally local mesh refinements are executed after model calibration to study the effects of river interventions. This study shows both the errors caused by bathymetry discretization and numerical effects for locally refined meshes. First, schematised river meanders with a flat bed in the transverse flow direction are analysed to isolate the induced numerical effects by the mesh. Afterwards, a case study is considered to verify if similar mesh influences are found in natural river meanders. Curvilinear, triangular and hybrid (combination of curvilinear and triangular cells) meshes are used with different resolutions. The analysis shows that in the schematised river meanders lower depth-averaged flow velocities and larger water depths are simulated with coarser meshes. In the case study, substantial differences in hydrodynamics between the meshes are obtained suggesting that the bathymetry discretization is more influential than the numerical effects. Finally, it was found that triangular meshes, and rivers with narrow meander bends, are most sensitive to mesh resolution. Especially in these cases, it is desirable to refine the mesh at the desired locations before model calibration.

KEYWORDS
bathymetry accuracy, mesh resolution, mesh shape, numerical effects, river meander, two-dimensional depth-averaged hydraulic model

1 | INTRODUCTION

A detailed insight into flow patterns in rivers is crucial as it helps analysing the impacts of river interventions regarding, for example, sediment management and flood protection. A common approach to investigate such processes is by making use of two-dimensional depth-averaged (2DH) hydraulic models since vertical motions are assumed to be insignificant and the water depths in rivers are relatively shallow compared to the width (Altaie & Dreyfuss, 2018; Lai, 2010; Hardy, Bates, & Anderson, 1999). Therefore, the Shallow Water Equations (SWEs) are generally used, which are given by the depth-averaged continuity equation and the momentum equations

(Section 2.1). In order to simulate flow pattern predictions with 2DH hydraulic models, study areas are discretized with meshes. Generally, fully curvilinear or fully triangular meshes are used to solve the governing equations in hydraulic river models. A combination of curvilinear and triangular mesh cells is also possible and is known as a hybrid mesh.

In the field of computational fluid dynamics (CFD), the optimum mesh resolution is generally found by performing a mesh convergence analysis (Tezdogan, Incecik, & Turan, 2016). In such an analysis, multiple model runs are performed with an increasing mesh resolution until a further increase in resolution does not result in a significant change in model output. However, due to computational time restrictions for large-scale river applications, hydraulic models commonly have mesh cell sizes in the order of +10 m. Consequently, the model output of such coarse 2DH river models is largely influenced by the mesh set-up in terms of mesh resolution and mesh shape (Bomers, Schielen, & Hulscher, 2019). Mesh coarsening and a poor alignment between the mesh and the direction of the flow lead to a smoothed hydrograph, resulting in lower depth-averaged flow velocities and higher water depths (Caviedes-Voullième, Garcia-Navarro, & Murillo, 2012). This mesh-generated effect has a diffusion-like appearance and is known as "numerical diffusion". This effect is a result of a truncation error and is induced when numerical algorithms, such as the upwind scheme, are used to solve the advection problem in the SWEs.

Another mesh-generated effect is the accuracy of the bathymetry discretization reflecting how well the digital elevation model (DEM) is schematised by the mesh. Typically, the bathymetry discretization accuracy is higher for high-resolution meshes. A mesh should be fine enough to capture important flow features and geometrical structures. Caviedes-Voullième et al. (2012) showed that small details in river bathymetry can sometimes affect large-scale flow behaviour. The outcomes of hydraulic river models largely depend on the bathymetry discretization since the river cross-sectional area can be overestimated and underestimated by low-resolution meshes, influencing the discharge capacity and consequently the simulated water levels (Bomers et al., 2019; Caviedes-Voullième et al., 2012).

Numerical diffusion and bathymetry discretization influence model outcomes in large-scale river models since relatively low mesh resolutions are used. Therefore, hydraulic models are generally calibrated by altering the channel roughness until the model output is close to measurements. As such, the channel roughness compensates for the mesh-related errors (Bomers et al., 2019) and these calibrated roughness values are mesh-dependent. However, to assess the impact of river interventions, meshes are commonly locally refined after model calibration at the intervention locations to accurately schematise the bathymetry, for example, to accurately simulate the discharge partitioning at the bifurcation point of a side channel (Ji & Zhang, 2019) or to simulate the effect of in-stream structures for river restoration to improve physical habitats (Theodoropoulos et al., 2020). However, a local mesh refinement results in a change of the numerical effects and re-calibration might be required. The effects of a local increase in mesh resolution are not yet fully understood as it is currently unknown to what extent a locally refined mesh in narrow and wide river bends influences model outcomes.

In Caviedes-Voullième et al. (2012) and Bomers et al. (2019), the importance of mesh resolution is discussed. In these studies, the influences of numerical diffusion and bathymetry discretization effects were interrelated as both studies considered case studies. Consequently, it is unclear to what extent numerical effects or the bathymetry accuracy impact hydraulic river modelling outcomes separately. Therefore, this study aims to understand how numerical effects and the accuracy of the bathymetry discretization affect model outcomes to identify if a local refinement of the mesh is appropriate after model calibration. We express model outcomes in terms of simulated water depths, water levels and depth-averaged flow velocity profiles in meander bends. To assess the model outcomes, we construct various meshes for both (1) schematised river meanders with a flat bed in the transverse flow direction to exclude the effects of bathymetry accuracy and (2) a case study where both numerical effects and bathymetry discretization influence model outcomes. A local mesh refinement is performed to determine its effects on local water depths and flow velocities.

The paper is organised as follows. Section 2 introduces the set-up of the hydraulic models of the case study and the schematised river meanders. Section 3 firstly presents the results of the schematised river meanders to solely consider the numerical effects. Next, the results of the case study are presented to also consider bathymetry discretization effects. Section 4 discusses the results of the considered cases. Section 5 presents the conclusions of the paper.

2 | METHODS

2.1 | Hydraulic model

2DH hydraulic modelling is performed with D-Flow Flexible Mesh (FM). The SWEs can be derived by depth-integrating the 3D Navier–Stokes equations:

$$\frac{\partial h}{\partial t}+\frac{\partial hu}{\partial x}+\frac{\partial hv}{\partial y}=0 \tag{1}$$

$$\underbrace{\frac{\partial hu}{\partial t}}_{1}+\underbrace{\frac{\partial hu^2}{\partial x}+\frac{\partial huv}{\partial y}}_{2}=\underbrace{-gh\frac{\partial \zeta}{\partial x}}_{3}+\underbrace{\nu\left[\frac{\partial}{\partial x}\left(h\frac{\partial u}{\partial x}\right)+\frac{\partial}{\partial y}\left(h\frac{\partial u}{\partial y}\right)\right]}_{4}+\underbrace{fhv}_{5}+\underbrace{\frac{\tau_u^w}{\rho}}_{6}+\underbrace{\frac{\tau_u^b}{\rho}}_{7} \tag{2}$$

$$\underbrace{\frac{\partial hv}{\partial t}}_{1}+\underbrace{\frac{\partial huv}{\partial x}+\frac{\partial hv^2}{\partial y}}_{2}=\underbrace{-gh\frac{\partial \zeta}{\partial y}}_{3}+\underbrace{\nu\left[\frac{\partial}{\partial x}\left(h\frac{\partial v}{\partial x}\right)+\frac{\partial}{\partial y}\left(h\frac{\partial v}{\partial y}\right)\right]}_{4}-\underbrace{fhu}_{5}+\underbrace{\frac{\tau_v^w}{\rho}}_{6}+\underbrace{\frac{\tau_v^b}{\rho}}_{7} \tag{3}$$

In the SWEs, t represents the time (s), u and v are the depth-averaged flow velocities (m/s) in respectively $x-$ and $y-$ direction, g is the gravitational acceleration (m/s^2), ζ is the water level (m), ν is the kinematic viscosity (m^2/s). ρ represents the density of the water (kg/m^3), which is assumed to be incompressible. f is the Coriolis frequency (rad/s). τ_u^b and τ_v^b are respectively bottom friction (N/m^2) in x-and y-direction. τ_u^w and τ_v^w are the wind friction acting at the free surface (N/m^2) in $x-$ and $y-$ direction respectively. Furthermore, it is important to recognise that the inertia, advection, hydrostatic pressure, diffusion, Coriolis force, wind and bottom friction terms are represented with, respectively, terms 1 until 7 in Equations (2) and (3).

2.2 | Case study: Grensmaas stretch

The Grensmaas, a stretch of the Meuse River, is used as a case study. The Grensmaas consists of both moderate and sharp meander bends with large local variations in floodplain width and is located between 15 and 55 km downstream from where the Meuse River enters the Netherlands (Figure 1). The model domain includes the main channel of the Meuse River and its floodplains. The general characteristics of the Grensmaas were taken from Huthoff, Ouwerkerk, Daggenvoorde, Snoek, and Voortman (2020). The main channel of the Grensmaas has a length of approximately 40 km and has an average width of 140 m. The river channel width varies a little. Both floodplains together are on average 6 m higher with respect to the main channel and have an average width of 1,110 m. The bottom friction of the Grensmaas was expressed as the Nikuradse coefficient with an average calibrated value of $0.15m$ in the main channel and $0.91m$ on the floodplains. A characteristic bed slope for the Grensmaas is $4.49e-04m/m$. The upstream boundary of the model domain was placed at Eijsden at km-2 while the downstream boundary was located upstream of the City Maasbracht at km-64 (Figure 1).

We evaluated two sub-reaches of the Grensmaas (Figure 1: red regions), one with almost no floodplains and one with wide floodplains, to compare the influence of a mesh structure on model outcomes. In order to evaluate the hydrodynamics in the transverse flow direction, we analysed the complete cross-sectional areas at the bend apexes in the two selected regions (Figure 1: CS 1 and CS 2).

An initial water level was set throughout the entire spatial domain which corresponds to a discharge of $250m^3/s$. At km-2, the system was forced with a semi-stationary discharge, which can be divided into two categories: (i) low-and (ii) high-range semi-stationary discharges. The model domain was initially forced with a low-range of $250m^3/s$ and was eventually increased to a high range of $3430m^3/s$ after three days. A predefined rating curve based on measurements and hydraulic model simulations was used to set up the downstream boundary condition at km-64.

2.3 | Schematised river meanders

The river characteristics of the schematised river meanders were chosen such that these correspond with those of the Grensmaas. In this way, we can relate the outcomes of the schematised river meanders with those of the case study. For the development of the schematised river meanders, we used the following river characteristics of the Grensmaas: (i) main channel width; (ii) floodplain width, which is half of the average total floodplains width; (iii) floodplain height with respect to the bed level of the main channel; (iv) river slope and (v) bottom friction in the main channel and floodplains.

We set up schematised river meanders based on the intrinsic function (Langbein & Leopold, 1966). The so-called sine-generated curve (Langbein & Leopold, 1966) describes the rate of change in direction along its path by a sinusoidal function. The angle between the meander curve and the horizontal is defined as the "direction angle" (θ). We adopted this theoretical approach since such curves are formulated to have the least average curvature per unit length. This results in the least total work needed for a fluid particle to accelerate (by changing its direction) through the river meander. Consequently, this leads to flow patterns that are comparable to those in a natural river meander (Langbein & Leopold, 1966).

To capture the extremes of these geometrical characteristics in the Grensmaas, we analysed three meander curves: (i) a moderate curve without floodplains; (ii) a sharp curve without floodplains and (iii) a sharp curve with floodplains (Figure 2). All schematised river meanders consisted of a total meander length of 30 km. Furthermore, a so-called "valley slope" of $4.49e-04m/m$ was applied, which is a slope along a straight line through the meander bends. In this way, identical bed levels were obtained over a specified distance in the horizontal direction for both the moderate and sharp meanders.

A constant initial water level of $0m$ with respect to the bed level of the main channel at $x=0$ was set throughout the entire spatial domains of the three schematised river meanders. At $x=0$, all three schematised river meanders were forced with a unique semi-stationary discharge until similar water levels are obtained between the schematised river meanders. We divided the forcing into two low and three high-range semi-stationary discharges. To obtain similar water levels, we used a low discharge range of 946 m^3/s for the moderate meander with no floodplains and 844 m^3/s for both the sharp meander with and without floodplains. For the high-discharge range, we used discharges of 3,002, 2,679 and 3,801 m^3/s for the moderate meander without floodplains, the sharp meander without floodplains and the sharp meander with floodplains, respectively. Each schematised case was initially forced with the low-range and was eventually increased to the high range after ten days. We used predefined rating curves based on steady uniform flow considerations for the downstream boundary conditions.

For the schematised river meanders, we reviewed the hydrodynamics in the second river bends simulated by various mesh structures

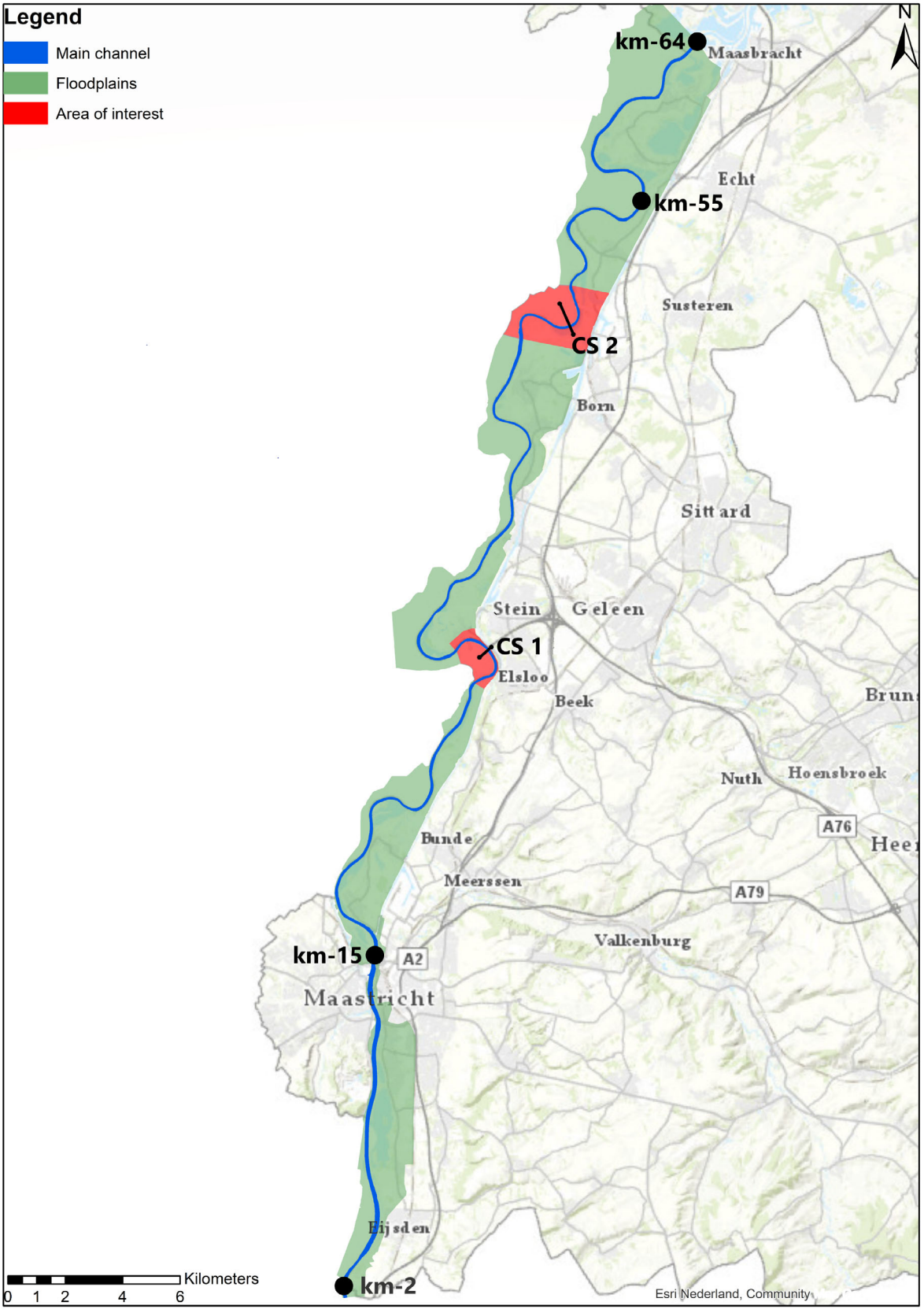

FIGURE 1 The study area. The model-domain ranges from km-2 Eijsden till km-64 (Maasbracht) in which the Grensmaas stretch is located between the trajectory km-15 and km-55. The blue and green colours represent respectively the main channel and floodplains. The computed hydrodynamics in the red regions are considered for the evaluation of the meshes. The black lines illustrate the cross-sectional areas we touch upon. [Color figure can be viewed at wileyonlinelibrary.com]

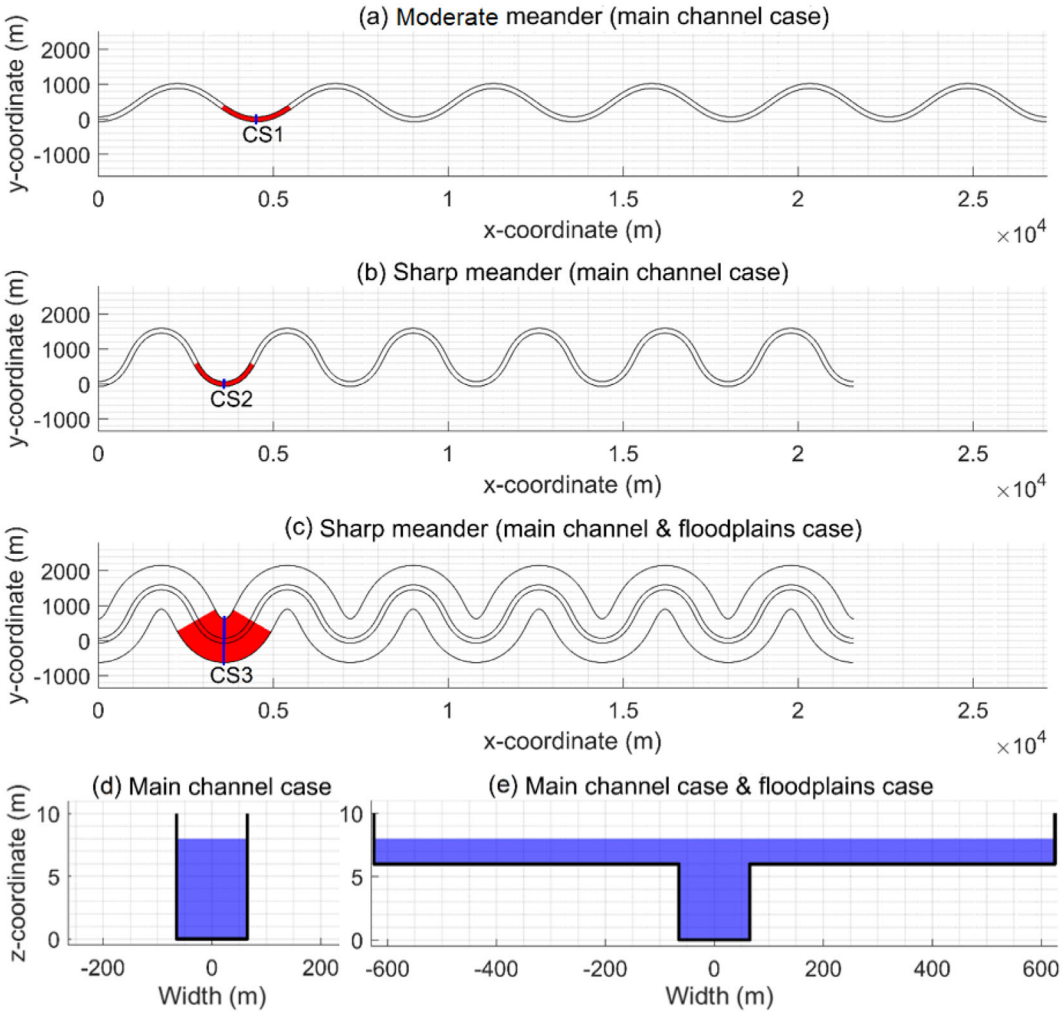

FIGURE 2 In (a–c) a top-view of the three schematised river meanders. The black lines represent the land boundaries. For the evaluation of the meshes, we consider the computed hydrodynamics in the red regions. The blue lines illustrate the cross-sectional areas we touch upon. In (d,e) the applied cross-sections in the schematised river meander cases with/without of floodplains. [Color figure can be viewed at wileyonlinelibrary.com]

since these regions are far away from the downstream boundary condition (Figure 2: red regions). To analyse the hydrodynamics in transverse flow direction within river bends, we evaluated the complete cross-sectional areas at the bend apexes (Figure 2: CS 1, CS 2 and CS 3).

2.4 | Computation scheme of the numerical meshes

To discretize the governing equations, we applied a finite volume method on a staggered scheme. Water levels are stored at the cell centres whereas velocity variables are found at the cell faces (Harlow & Welch, 1965; Tu, Yeoh, & Liu, 2013). This approach differs from a collated arrangement, in which all SWEs variables are discretized at the same positions (Meier, Alves, & Mori, 1999; Mungkasi, Magdalena, Pudjaprasetya, Wiryanto, & Roberts, 2018; Tu et al., 2013). According to Stelling (1983), a staggered scheme is a more effective discretization method for the SWEs as the number of mesh points is reduced by a factor four in comparison to a collocated scheme reducing the computation time.

Triangular and hybrid meshes have gained much attention over the recent years due to the flexibility they provide in complex geometries. For computational efficiency, we used orthogonal grids such that the pressure gradients only depend on two pressure points, which reduces computation time and results in higher model accuracy (Kleptsova, Pietrzak, & Stelling, 2009). The orthogonality principle enforces the criteria that the corners of two adjacent grid cells are placed on a common circle and that the line segment, which connects the circumcenter of two neighbouring cells, intersects orthogonally with the interface between them (Bomers et al., 2019; Casulli & Walters, 2000; Kernkamp, Dam, Stelling, & Goede, 2011; Kleptsova et al., 2009). In this study, we aimed for a maximum deviation of 2 from perfectly orthogonal mesh cells (90°) (Minns, Spruyt, & Kerkhoven, 2019).

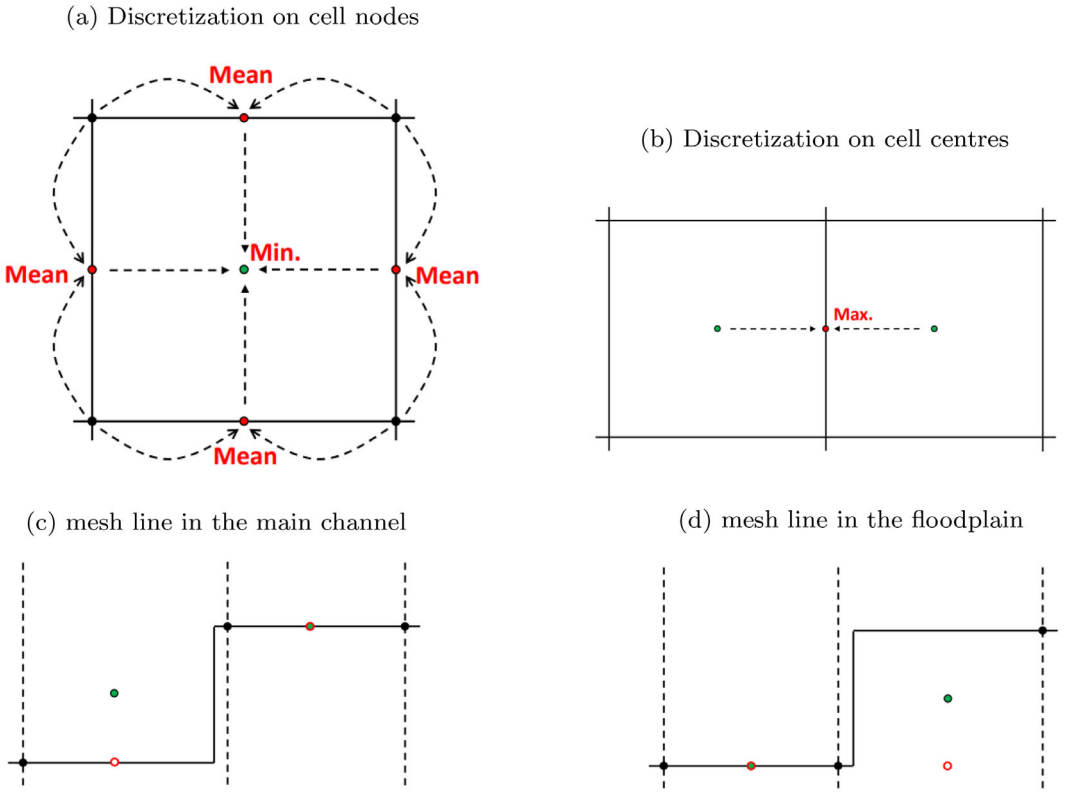

FIGURE 3 In (a,b) an illustration of how the bed level is discretized in respectively with the main channel and the cases with the main channel and floodplains. The filled black circles and solid black lines represent respectively the nodes and borders of the mesh cells. The bed level at the cell faces is computed at the red-filled circles. The bed level of a mesh cell at the mesh centre is symbolised with green-filled dots. In (c,d) a cross-section view of the bed level in the case of the schematised river meanders with floodplains. The original bed level is given by the solid black lines, whilst the mesh lines are represented by the dotted black line. The bed level at the mesh nodes and cell faces are given by the black and green-filled circles, respectively. The red circles denote the bed level at the cell centre positions. (c) illustrates an increase in the discharge capacity of the main channel when the bed level is discretized on the mesh nodes, whereas (d) results in a lower discharge capacity (De Jong, 2020). [Color figure can be viewed at wileyonlinelibrary.com]

In terms of the discretization of the bathymetry, we discretized the bed levels on the corner nodes of the mesh cells in the schematised river meanders where floodplains are not included (Figure 3a). The bed level at the cell faces was then defined by the mean between the two corner nodes of a mesh cell (Figure 3a). Eventually, the lowest mean-values between two corner nodes determine the bed level at the cell center of a mesh cell (Figure 3a) (Deltares, 2019).

Due to the clear distinction between the main channel and floodplains, another set-up is required in the schematised case with floodplains. Otherwise, due to the large discretization errors of the bathymetry, significant differences in simulated hydrodynamics would have been obtained (see Figure 3c,d). Therefore, the bed levels were projected directly at the cell centre (Figure 3b). Consequently, the bed level at the cell faces was then defined by the maximum bed level of two adjacent mesh cells (Figure 3b) (Deltares, 2019).

For the case study, the bed levels were discretized on the corner nodes. If the bed levels are projected at the cell centers, an overestimation of the bed levels at the cells faces can be expected due to the river slope (De Jong & Yossef, 2016). Furthermore, more gradual transitions between the main channel and the floodplains occur in the case study, which makes the discretization on the cell nodes applicable. However, we briefly considered the differences in bed level at the transition. There are two options for the mesh generation: (i) placing the mesh lines at the transition between the main channel and floodplains on the lower-lying ground (Figure 3c); or (ii) placing the mesh lines at the transition in the floodplains (Figure 3d). In the hydraulic model, bed levels at the cell centre define the water storage in a mesh cell. The flow area to the neighbouring cell on the other hand is determined by the bed levels at the cell faces. Consequently, we obtain an overestimation and underestimation of the flow area with respectively the set-up in Figure 3c,d. Since the water level in the river largely depends on the flow area, it is essential to simulate this properly. Therefore, the mesh lines were placed in the main channel of the Grensmaas, while a steep transition between the main channel and floodplains (slope steeper than 1 : 7) was modelled by defining it as a fixed weir (Hoefsloot & Van Doornik, 2020). A crest level was assigned to the fixed weirs corresponding to the height of the floodplain (De Jong, 2020).

TABLE 1 Properties of the constructed grids for the schematised river meanders with only the main channel

Moderate & sharp river meander (main channel case)		
Name	**Mesh shape**	**Number of mesh cells across MC**
M_MC_Cur_HR	Curvilinear	20
S_MC_Cur_HR		
M_MC_Cur_LR	Curvilinear	5
S_MC_Cur_LR		
M_MC_Tri_HR	Triangular	8
S_MC_Tri_HR		
M_MC_Tri_LR	Triangular	3
S_MC_Tri_LR		
Sharp river meander (main channel & floodplains case)		
Name	Mesh shape	Number of mesh cells across MC
S_MCFL_Cur_HR	Curvilinear	20
S_MCFL_Cur_LR	Curvilinear	10
S_MCFL_Hybr_HR	Curvilinear in MC; triangular in FL	20
S_MCFL_Hybr_LR	Curvilinear in MC;	10
	Triangular in FL	
S_MCFL_Tri_HR	Triangular	8
S_MCFL_Tri_LR	Triangular	4
Case study: Grensmaas stretch		
Name	Mesh shape	Number of mesh cells across MC
Grensmaas_Cur_HR	Curvilinear in MC; quadrilateral in FL of sharp bends	Min. 16
Grensmaas_Cur_LR	Curvilinear in MC; quadrilateral in FL of sharp bends	Min. 8
Grensmaas_Cur_LR_Loc_Ref	Curvilinear in MC; quadrilateral in FL of sharp bends; triangular at TRANS	Min. 8 (min. 16 loc. Ref.)
Grensmaas_Hybr_HR	Curvilinear in MC; triangular in FL	20
Grensmaas_Hybr_LR	Curvilinear in MC; triangular in FL	10
Grensmaas_Hybr_LR_Loc_Ref	Curvilinear in MC; triangular in FL and at TRANS	10 & (20 loc. Ref.)
Grensmaas_Tri_HR	Triangular	Min. 6
Grensmaas_Tri_LR	Triangular	Min. 3
Grensmaas_Tri_LR_Loc_Ref	Triangular	Min. 3 & (min.6 loc. Ref.)

Note: Regarding the names: M and S stand respectively for moderate and sharp; MC for main channel; MCFL for main channel & floodplains; Cur, Tri and Hybr for respectively curvilinear, triangular and hybrid; and HR and LR for high and low resolution, respectively. Furthermore, FL stands for floodplains, TRANS for the shifts between the low-resolution variant and local refinements, and Loc & Ref for locally and refined, respectively.

2.5 | Meshes

Several meshes were constructed to analyse the influence of different mesh shapes and mesh resolutions on hydraulic modelling outcomes. Here, we present the meshes for the schematised river meanders and the Grensmaas respectively followed by the locally refined meshes for the Grensmaas.

2.5.1 | Meshes for schematised river meanders

Curvilinear and triangular meshes are considered with two different mesh resolutions in the main channel of both the moderate and sharp schematised river meanders (Table 1 and Figure 4a–c):

- Curvilinear high-resolution mesh: a curvilinear mesh was used with 20 mesh cells in the transverse flow direction. The mesh cells were aligned in the flow direction such that they follow the river course.
- Curvilinear low-resolution mesh: the set-up is similar to the high-resolution variant, but now with 5 mesh cells in the transverse flow direction.
- Triangular high-resolution mesh: 8 mesh cells were placed in the transverse flow direction to ensure the same number of mesh cells within the model domain as the high-resolution curvilinear mesh.
- Triangular low-resolution mesh: the set-up is similar to the high-resolution variant, but now with 3 mesh cells in the transverse flow direction.

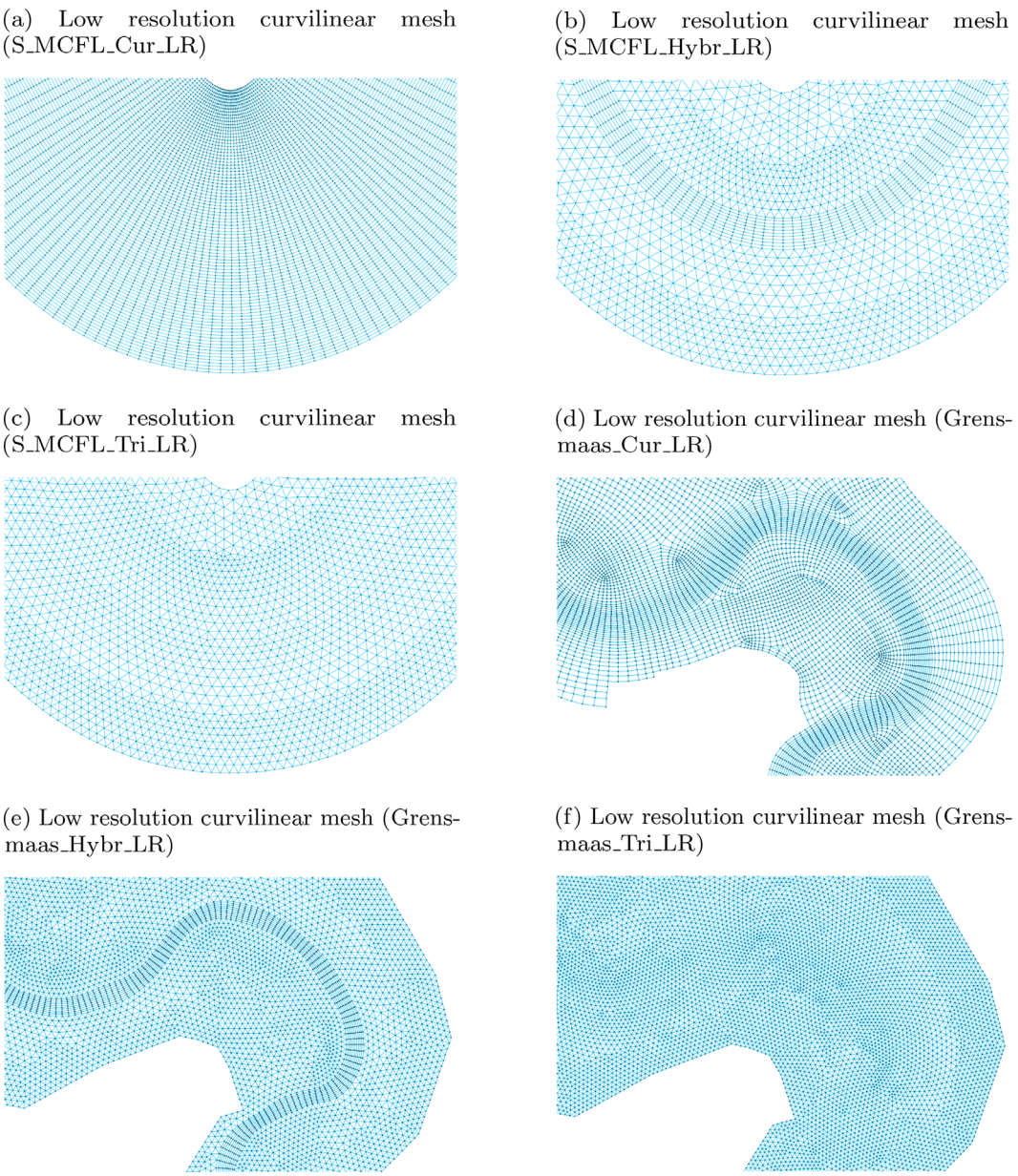

FIGURE 4 In (a–c) an illustration of three low-resolution meshes in the second bend of the schematised sharp river meander with floodplains. In (d–f) an illustration of three low-resolution meshes for the Grensmaas in the narrow river bend with almost no floodplains (see Figure 1). The names of the meshes are provided between brackets where S refers to sharp; MCFL to main channel & floodplains; Grensmaas refers to Grensmaas stretch; Cur, Hybr and Tri to respectively curvilinear, hybrid and triangular; and LR for the low-resolution variants. [Color figure can be viewed at wileyonlinelibrary.com]

In the schematised case when floodplains were incorporated, only a sharp meander bend was considered. For this case, curvilinear, triangular and hybrid meshes were used, with again a high and low-resolution variant (Table 1 and Figure 4a–c):

- Curvilinear high-resolution mesh: 20 mesh cells in the transverse flow direction were used in the main channel. The mesh was aligned in the direction of the river course with a clear transition between the main channel and floodplain to accurately capture the bathymetry. Smaller width-length (aspect) ratios were considered in the main channel compared to the cases without floodplains to prevent the aspect rations becoming smaller than one at the inner bend of the floodplains, having a negative effect on computation times.
- Curvilinear low-resolution mesh: the set-up is similar to the high-resolution variant, but now with 10 mesh cells in the main channel.
- Triangular high-resolution mesh: 8 mesh cells in the transverse flow direction were used in the main channel. To set up this mesh, first the main channel was discretized where after we focused on the discretization of the floodplains to acquire a clear transition

between the main channel and floodplains. To generate the triangular meshes in the floodplains, we used the net links positioned at the boundary of the triangular mesh in the main channel to connect a single triangular mesh cell in a floodplain with each triangular mesh cell in the main channel. This mesh generation strategy is known as "alignment with the flow direction" and results in triangular meshes which are structurally well-oriented with the main channel course (Bomers et al., 2019). Moreover, we obtained a good representation of the bathymetry because of the positioning of the net links at the boundary of the main channel.

- Triangular low-resolution mesh: the set-up is similar to the high-resolution variant, but now with 4 mesh cells in the main channel.
- Hybrid high-resolution mesh: a curvilinear mesh was used in the main channel with 20 mesh cells in the transverse flow direction. The floodplains were discretized with a triangular mesh such that each triangular mesh cell at the main channel-floodplain boundary is connected to one curvilinear mesh cell.
- Hybrid low-resolution mesh: the set-up is similar to the high-resolution variant, but now with 10 mesh cells in the main channel.

2.5.2 | Meshes for the Grensmaas

Similar mesh structures were constructed for the Grensmaas as for the schematised case with floodplains (Table 1 and Figure 4d–f). However, slight adjustments were made to the curvilinear mesh which now discretizes the model domain with as many curvilinear mesh cells as possible. At sharp river bends (with floodplains), quadrilateral (a polygon with four edges or sides and four vertices or corners) mesh cells are included to prevent overlapping small mesh cells in the sharp and large floodplains of the Grensmaas. Additionally, the transverse mesh resolution of the adjusted curvilinear mesh in the floodplains decreases exponentially with a factor 1.05. In terms of the mesh resolution of the curvilinear, triangular and hybrid meshes, we again examined a high and low mesh resolution. The resolutions of these meshes are in line with the meshes for the schematised river meanders.

2.5.3 | Meshes for the Grensmaas with local refinements

To gain a better understanding of how a local increase in mesh resolution influences hydraulic river modelling outcomes in the case study, we considered two local mesh refinements for each constructed low-resolution mesh (Table 1). A local mesh refinement was implemented in an area with narrow floodplains (Figure 1: around CS 1) and wide floodplains (Figure 1: around CS 2). For each mesh shape, the local refinements had the same resolution as the higher resolution variants.

In order to prevent mesh cells being connected to more mesh cells than the number of its net links, we applied triangular mesh cells at the transition between the low resolution and the locally refined regions. However, applying triangular mesh cells at the transition is at the expense of the orthogonality and smoothness criteria (ratio of the areas of the two adjacent mesh cells) of the locally refined curvilinear mesh due to the exponentially increasing mesh cell dimensions towards the outer edges of the floodplains. Therefore, the cell dimensions were gradually increased using quadrilateral mesh cells ensuring that the smoothness criteria were met between the low-resolution mesh and the locally refined regions.

3 | RESULTS

3.1 | Schematised river meanders

The following section presents the results of the schematised moderate river meander without floodplains followed by the sharp river meander without and with floodplains respectively as this order helps to isolate the induced numerical effects.

3.1.1 | Moderate river meander (main channel)

In the moderate river meander, it was found that the four meshes predicted more or less similar flood patterns: (i) an elevated water surface near the outer bank at the bend apex (Figure 5a); and (ii) higher depth-averaged flow velocities close to the inner bank just downstream of the bend entrance (Figure 6a–d).

However, larger water depths were predicted by the coarser curvilinear and triangular meshes (Figure 5a). Furthermore, we observed greater differences between the minimum and maximum depth-averaged velocities through the river bend with the high-resolution variants of both mesh shapes (Figure 6a–d). A more diffused (uniform) depth-averaged flow velocity profile was predicted by the coarser meshes, which illustrates the influence of the numerical diffusion. With the lower discharge range, we found the same differences between the meshes, but to a lesser extent.

In terms of the differences between the mesh shapes, larger water depths and lower depth-averaged flow velocities were obtained with the high-resolution triangular mesh than with the high-resolution curvilinear mesh (Figures 5a and 6a–d). The opposite occurred for the low-resolution variants as the lowest resolution triangular mesh simulated lower water depths and higher maximum depth-averaged flow velocities (Figure 5a and 6a–d).

When applying coarser meshes, larger water depth and depth-averaged flow velocity differences were obtained than when using a different mesh shape indicating that mesh resolution had a larger effect on model outcomes than mesh shape.

3.1.2 | Sharp river meander (main channel)

In comparison to the more moderate river meander, we obtained similar flood patterns using all four meshes in the sharp river meander (Figure 5b and 6e–h). In terms of the differences between the meshes, larger water depths and lower depth-averaged flow velocities were

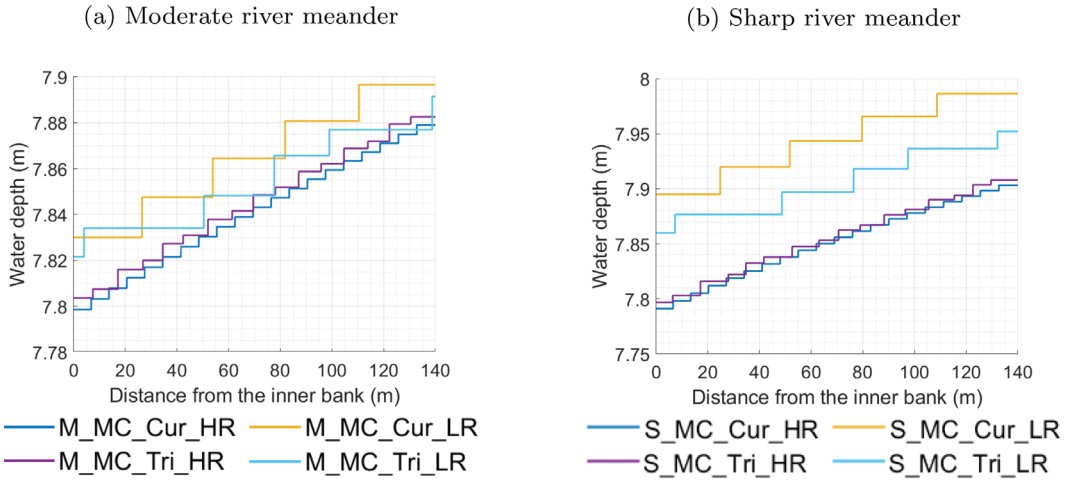

FIGURE 5 Cross-sectional view of the simulated water depth for the moderate and sharp river meander (main channel cases) with the highest discharge range at CS 1 and CS 2 by the four considered meshes for each river meander. Regarding the names: M and S stand for moderate and sharp; MC for main channel; Cur and Tri for respectively curvilinear and triangular; and HR and LR for high and low resolution, respectively. [Color figure can be viewed at wileyonlinelibrary.com]

simulated with the coarser meshes (Figure 6e–h). However, in the sharper bend greater differences in depth-averaged flow velocities were predicted between the inner and outer bend using the four meshes compared to the more moderate bend.

3.1.3 | Sharp river meander (main channel & floodplains)

In the schematised sharp river meander with floodplains, substantial differences in depth-averaged flow velocities were found at the inner bank, in the main channel and at the transition between main channel and floodplain areas (Figure 7a). Due to the rapid flow changes at the transition between main channel and floodplains, a clear diffusion-like appearance was visible around the transition. This appearance was more visible for coarser meshes as larger mesh cells result in more numerical diffusion (Figure 7a). However, contrary to the main channel cases, minor differences were obtained between the simulated water levels over the entire spatial domain by the six meshes (Figure 7b). The flow velocity differences were small, especially on the floodplains. Due to the effect of the floodplains, the induced numerical effects in the main channel and at the transition with the floodplains were distributed throughout the model domain and hence dampened.

3.2 | Case study: Grensmaas

3.2.1 | Numerical and bathymetry discretization effects

Similar to the schematised river meanders, higher water levels were simulated by the coarser variants of the curvilinear, hybrid and triangular meshes for the highest discharge range in the narrow river bend (Figure 8a). Nonetheless, in comparison to the schematised river meanders, substantially larger water level and depth-averaged flow velocity differences were obtained between the meshes in the case study (Figure 8). In addition, significant differences in water levels and depth-averaged flow velocities between the meshes were found at the lower discharge range (Table 2).

With respect to the mesh shapes, the curvilinear and hybrid meshes predicted comparable depth-averaged flow velocities and water levels under the same level of mesh resolution. Under the same mesh resolution, water level differences between the curvilinear and hybrid meshes ranged $0-5cm$ when considering both the low and high discharge scenarios. The triangular meshes predicted substantially higher water levels, where the differences between the curvilinear meshes with comparable mesh resolutions ranged $9-87cm$. This indicates that a higher resolution was required with the triangular meshes in order to achieve the same level of accuracy as the curvilinear and hybrid meshes.

Less depth-averaged flow velocity differences were found between the meshes in the floodplain areas of the wide river bend (Figure 8c,d). Consequently, throughout the river bend with wide floodplains, relatively smaller differences in depth-averaged flow velocities were obtained between the meshes compared to the narrow river bend. Therefore, due to the large floodplain effect, bathymetry discretization and numerical effects which were predominantly induced in the main channel were distributed throughout the model domain and hence dampened. These findings were in line with the results of the schematised sharp river meander with floodplains.

3.2.2 | Impact of local mesh refinements

When considering the local mesh refinements, the simulated water levels at the bend apex CS 1 converged towards those of the higher

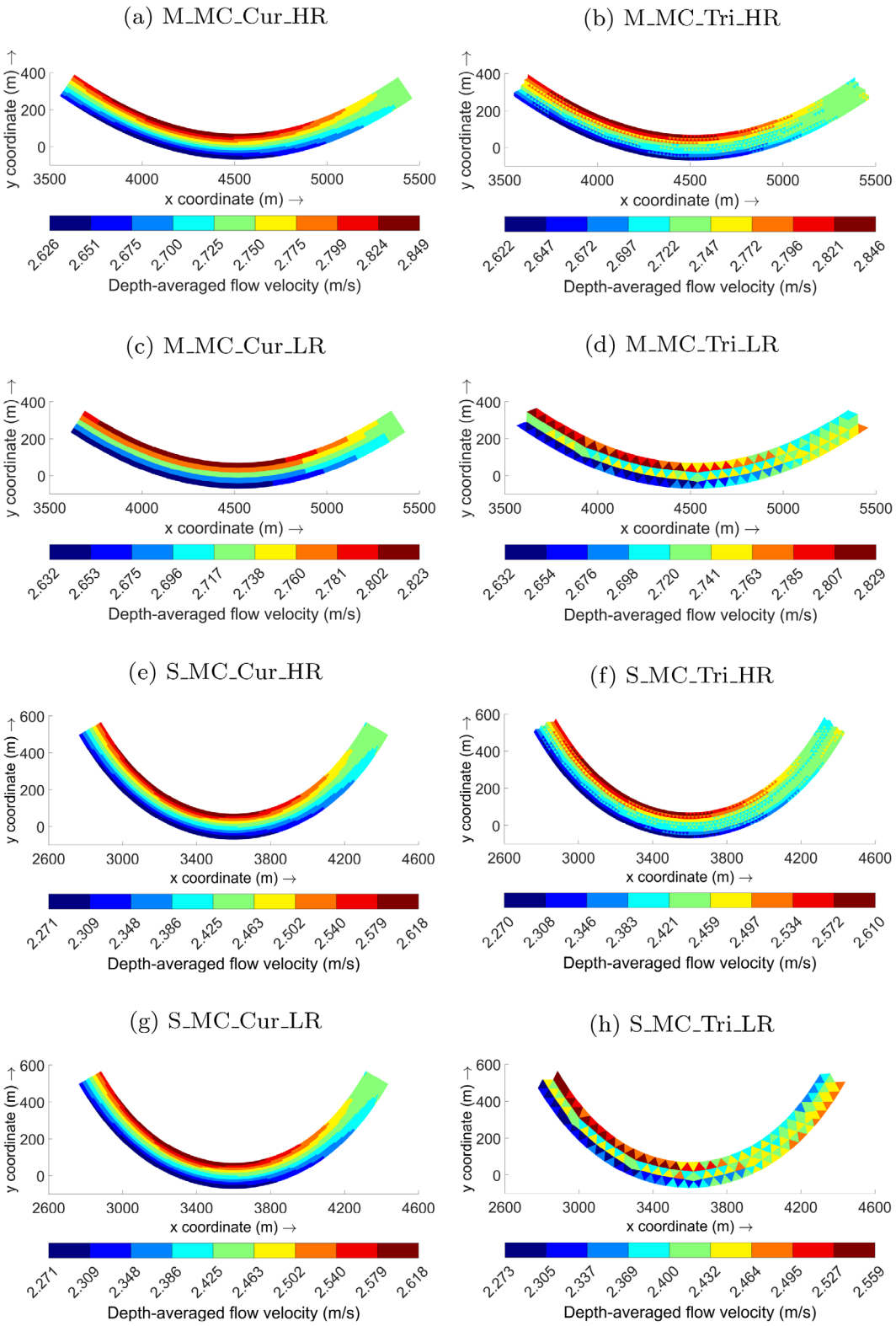

FIGURE 6 Map-plots of the simulated depth-averaged flow velocities for the moderate and sharp river meander (main channel cases) with the highest discharge range by the four considered meshes for each river meander. Regarding the names: M and S stand for moderate and sharp; MC for main channel; Cur and Tri for respectively curvilinear and triangular; and HR and LR for high and low resolution, respectively. [Color figure can be viewed at wileyonlinelibrary.com]

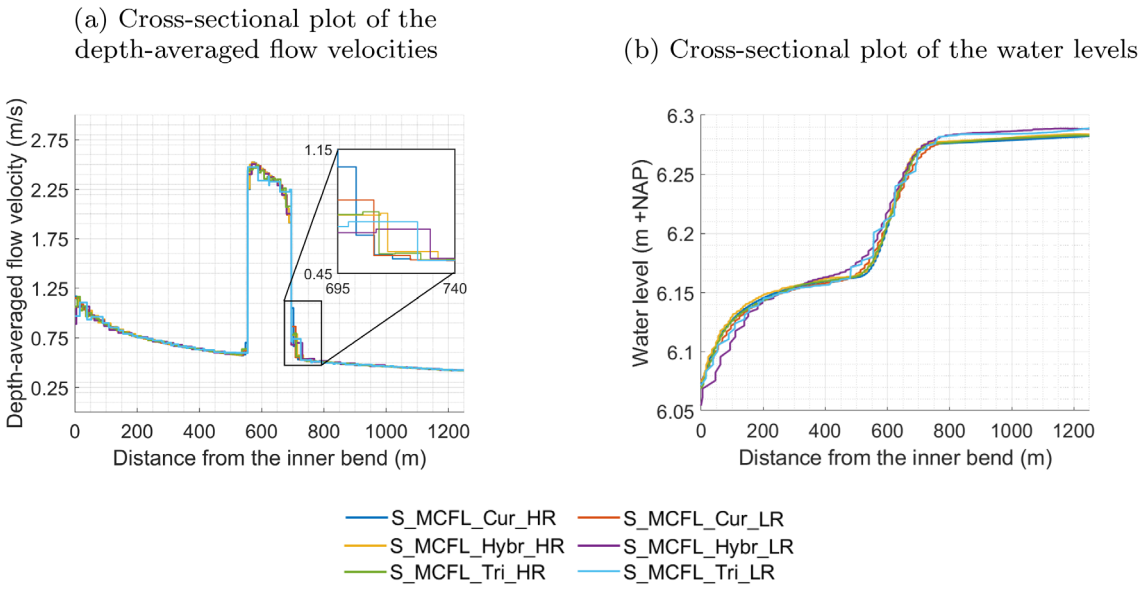

FIGURE 7 Cross-sectional view of the simulated water level and depth-averaged flow velocities in the schematised sharp river meander (main channel and floodplain case) for the highest discharge range at CS 3 by the six considered meshes. Regarding the names: S stands for sharp; MCFL for main channel & floodplains; Cur, Tri and Hybr for respectively curvilinear, triangular and hybrid; and HR and LR for high and low resolution, respectively. [Color figure can be viewed at wileyonlinelibrary.com]

resolution variants (Table 2). The latter was especially the case for the Grensmaas_Cur_LR_Loc_Ref and Grensmaas_Hybr_LR_Loc_Ref. The water levels simulated by the Grensmaas_Tri_LR_Loc_Ref converged towards water level values predicted by Grensmaas_Tri_HR as well. However, the simulated water levels at CS 1 by the former deviated significantly compared to the latter mesh. This indicated that curvilinear and hybrid meshes were more responsive to local mesh refinements than triangular meshes.

Similar results were obtained in the wide river bend (Table 2). However, in comparison to the narrow river bend, water levels simulated by the Grensmaas_Tri_LR_Loc_Ref became closer to those of the higher resolution variant. This can be explained by the dampening effect of wide floodplains, which led to overall closer water level predictions by all six meshes.

The outcomes in both the wide and narrow river bends showed that a local mesh refinement was an effective technique to reduce the effects of the bathymetry discretization locally since the water levels and flow velocities converged towards those simulated by the higher resolution meshes. However, since the discretized bathymetry between the locally refined meshes was different from that of the previous low-resolution meshes, affecting the river's discharge capacity, re-calibration of the model is required. Therefore, we advise first carrying out the local mesh refinement before executing the calibration procedure. During the calibration, the roughness coefficient will be altered to compensate for, among others, errors in the discretized bathymetry. Therefore, the calibrated roughness coefficients for the low-resolution mesh should not be applied to a locally refined mesh. This especially applies to triangular meshes and river sections with narrow meander bends since these were found to be most sensitive to a change in mesh resolution compared to triangular meshes and wide meander bends. It can be time consuming to calibrate various meshes after each local mesh refinement if the effect of multiple river interventions must be studied. However, strictly speaking, this is the correct way to obtain a fair indication of the effect of a river intervention on local water levels which is highly important in the light of designing appropriate flood protection measures.

4 | DISCUSSION

In this study, we simulated the hydrodynamics in the schematised river meanders and the Grensmaas with different mesh shapes and mesh resolutions. In the schematised river meanders, water depth differences varied in the order of millimeters to centimetres between the various meshes. For the Grensmaas on the other hand, we found substantially larger water level differences which varied in the order of centimetres to decimetres. The latter findings correspond well with the case studies of Mohamad, Lee, and Raksmey (2016) and Bomers et al. (2019), who both observed water level differences in the same order of magnitude. Caviedes-Voullième et al. (2012) on the other hand claimed that the numerical effects can be as influential as physical friction. However, in the study by Caviedes-Voullième et al. (2012), the effects of the bathymetry discretization were mixed with the numerical effects, since only a case study was considered. From these findings, we conclude that the bathymetry discretization primarily influences model outcomes since it determines the river's discharge capacity, while numerical diffusion only has a limited effect on model outcomes.

The hydraulic simulations were performed in D-Flow Flexible Mesh (FM). However, various alternative software programs exist such as MIKE21 FM and SRH-2D. Both adopt a flexible mesh

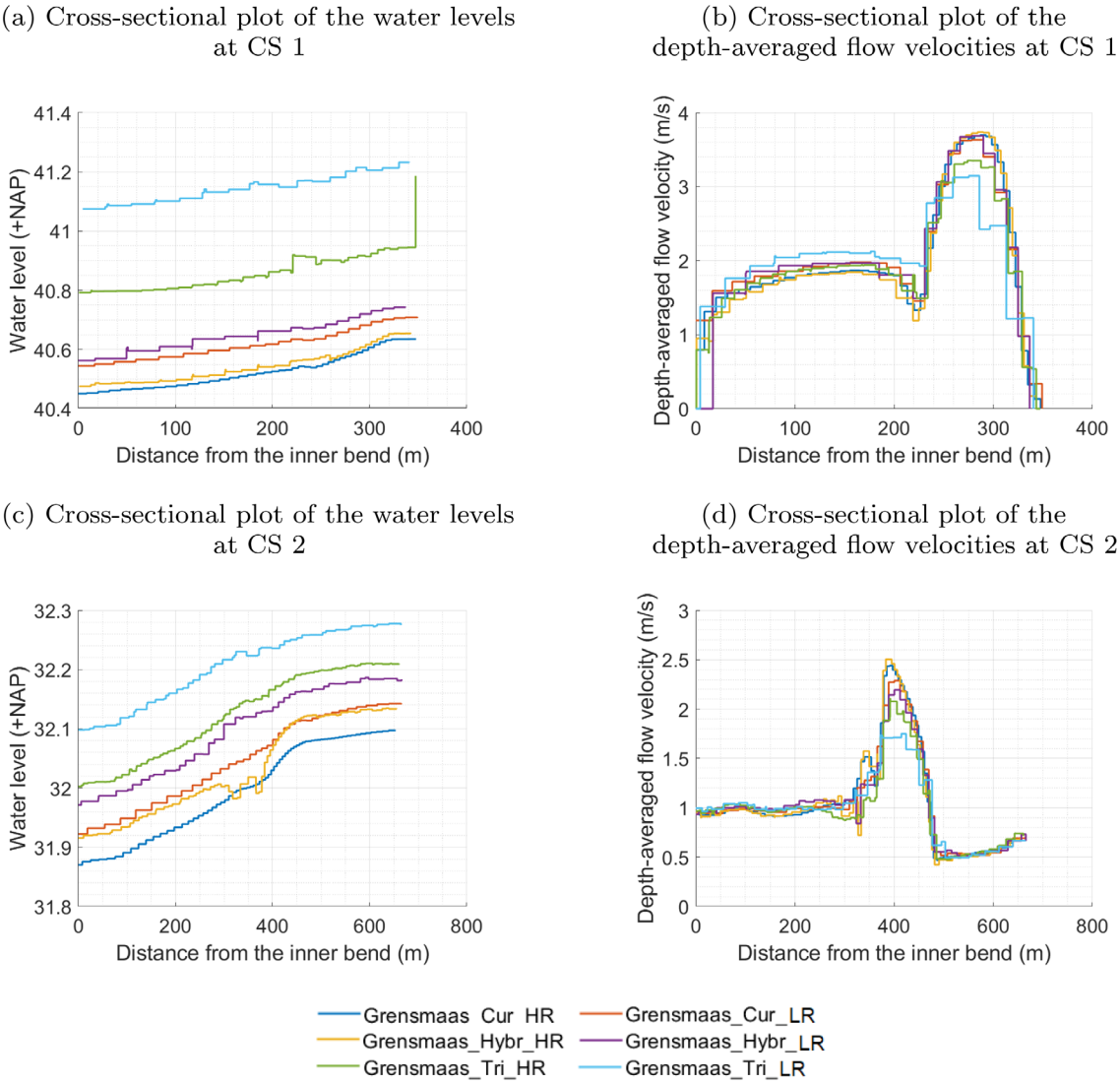

FIGURE 8 Cross-sectional view of the simulated water levels and depth-averaged flow velocities for the highest discharge range at CS 1 and CS 2. Regarding the names: Grensmaas stands for the Grensmaas stretch; Cur, Tri and Hybr for respectively curvilinear (as much as possible), triangular and hybrid; and HR and LR for high and low resolution, respectively. [Color figure can be viewed at wileyonlinelibrary.com]

clustering approach like D-Flow FM. In Lai (2010), the hydrodynamics through a 90◦ meandering flume was simulated with SRH-2D. The results corresponded well with our study as it was found that for triangular meshes, a higher resolution was required in order to obtain the same level of accuracy as the curvilinear meshes. In Parsapour-Moghaddam, Rennie, and Slaney (2018), both D-Flow FM and MIKE21 FM were used for hydraulic simulations of a meandering section of the Bow River, Canada. They found that lower depth-averaged flow velocities and higher water levels were obtained by the triangular mesh, which is in line with our findings for the Grensmaas. Therefore, it is presumed that the findings of this study also hold for other natural river meanders and other alternative hydrodynamic simulation software programs such as MIKE 21 FM and SRH-2D.

Regarding the evaluation of the effectiveness of river interventions (e.g., flood mitigation strategies), calibrating the model based on this future scenario was not possible since historical data was required to perform the calibration procedure, which in the case of a river intervention is only available after the realisation of such an intervention (Berends, Straatsma, Warmink, & Hulscher, 2019). Therefore, we advise to first execute a local mesh refinement at the location of the future river intervention. Ideally, this mesh refinement should have a sufficiently high resolution such that the river's cross section is accurately captured. This mesh can be calibrated based on the current bathymetry by altering the bed roughness until the model output is close to measurements to compensate for the numerical effects and the errors caused by the relatively low-resolution mesh in the remaining parts of the model domain. These calibrated roughness values can then be used in the model including the updated bathymetry with intervention to limit the introduction of additional mesh effects.

TABLE 2 Predicted water levels in the main channel at the bend apexes (CS 1 & CS2) for the two discharges ranges by the three locally refined meshes

		Water level low-range (m + NAP)	Water level high-range (m + NAP)
CS1	Grensmaas_Cur_HR	34.51	40.57
	Grensmaas_Cur_LR_Loc_Ref	34.57	40.58
	Grensmaas_Cur_LR	34.61	40.67
	Grensmaas_Hybr_HR	34.53	40.60
	Grensmaas_Hybr_LR_Loc_Ref	34.56	40.61
	Grensmaas_Hybr_LR	34.62	40.71
	Grensmaas_Tri_HR	34.61	40.88
	Grensmaas_Tri_LR_Loc_Ref	34.77	41.04
	Grensmaas_Tri_LR	35.08	41.15
CS2	Grensmaas_Cur_HR	25.19	32.07
	Grensmaas_Cur_LR_Loc_Ref	25.22	32.11
	Grensmaas_Cur_LR	25.33	32.11
	Grensmaas_Hybr_HR	25.16	32.11
	Grensmaas_Hybr_LR_Loc_Ref	25.20	32.13
	Grensmaas_Hybr_LR	25.33	32.16
	Grensmaas_Tri_HR	25.37	32.19
	Grensmaas_Tri_LR_Loc_Ref	25.70	32.20
	Grensmaas_Tri_LR	26.20	32.25

Note: Regarding the names: Grensmaas stands for the Grensmaas stretch; Cur, Tri and Hybr for respectively curvilinear (as much as possible), triangular and hybrid; HR and LR for high and low resolution, respectively; and Loc and Ref for locally and refined, respectively.

5 | CONCLUSION

In this study, our objective was to assess the influence of mesh characteristics on the hydraulic outcomes of river meander models. We assessed the numerical effects by constructing various meshes for schematised river meanders with a flat bed in the transverse flow direction. The results showed that the numerical effects were proportional to mesh cell sizes, depth-averaged flow velocity, rapid flow changes and the orientation of the mesh lines with respect to the flow direction. The latter two factors were more pronounced in sharper bends. In a more realistic case study, we examined the combined effect of the numerical diffusion, false diffusion and the bathymetry discretization. The results of the case study demonstrated that the differences in simulated hydrodynamics become significantly greater between meshes when variations in bed levels were considered. Therefore, we conclude that the bathymetry discretization effects were more important than the numerical effects.

In contrast to narrow river sections, simulated water level differences became substantially smaller between meshes if large floodplains were included in both the schematised river meander as well as in the Grensmaas. The results showed that due to the presence of wide floodplains, relatively smaller depth-averaged flow velocities were obtained through the river bends in comparison to narrower river sections. As a result of a large floodplain effect, mesh-generated effects in the main channel were less pronounced and hence dampened throughout the river cross-section. Therefore, we conclude that mesh-generated effects are proportional to the discharge per unit width.

To assess the impact of a local mesh refinement on the outcomes of the 2D depth-averaged model, we refined two river bends in the Grensmaas. The results demonstrated that a local increase in mesh resolution contributes to converging water levels and depth-averaged flow velocities towards those of the higher resolution variants locally. It is recommended to first refine a certain part of the mesh before calibrating the model. Refining a mesh after calibration results in having calibrated roughness coefficients that correspond with those of the non-refined mesh. This recommendation especially applies to triangular meshes, and to rivers with narrow meander bends, since mesh resolution has a significant effect on model output in these situations.

ACKNOWLEDGEMENTS

This research is embedded in Netherlands Organisation for Scientific Research project 14506 which is partly funded by the Ministry of Economic Affairs and Climate Policy. Furthermore, the authors would like to thank the Dutch Ministry of Infrastructure for providing the data. Additionally, the authors would like to thank Mr. J. de Jong from Deltares for his valuable insights.

DATA AVAILABILITY STATEMENT

The D-Flow FM Meuse River model, used as a case study, is available on the Riverlab webpage (https://oss.deltares.nl/nl/web/riverlab-models).

ORCID

Anouk Bomers https://orcid.org/0000-0002-1560-6828

REFERENCES

Altaie, H., & Dreyfuss, P. (2018). Numerical solutions for 2d depth-averaged shallow water equations. *International Mathematical Forum*, *13*, 79–90. https://doi.org/10.12988/imf.2018.712102

Berends, K., Straatsma, M., Warmink, J., & Hulscher, S. (2019). Uncertainty quantification of flood mitigation predictions and implications for interventions. *Natural Hazards and Earth System Sciences*, *19*(8), 1737–1753. https://doi.org/10.5194/nhess-19-1737-2019

Bomers, A., Schielen, R., & Hulscher, S. (2019). The influence of grid shape and grid size on hydraulic river modelling performance. *Environmental Fluid Mechanics*, *19*(5), 1273–1294. https://doi.org/10.1007/s10652-019-09670-4

Casulli, V., & Walters, R. A. (2000). An unstructured grid, three-dimensional model based on the shallow water equations. *International Journal for Numerical Methods in Fluids*, *32*(3), 331–348. https://doi.org/10.1002/(SICI)1097-0363(20000215)32:3<331::AID-FLD941>3.0.CO;2-C

Caviedes-Voullième, D., Garcia-Navarro, P., & Murillo, J. (2012). Influence of mesh structure on 2d full shallow water equations and scs curve number simulation of rainfall/runoff events. *Journal of Hydrology*, *448–449*, 39–59. https://doi.org/10.1016/j.jhydrol.2012.04.006

De Jong, J. S. (2020). *Ontwikkeling zesde-generatie maas-model. modelbouw, kalibratie en validatie (concept)* (p. 1). Delft: Tech. Rep., Deltares, Boussinesqweg.

De Jong, J. S., & Yossef, M. (2016). *Riviermodellen in d-hydro - pilot-applicatie rijntakken* (p. 1). Delft: Tech. rep., Deltares, Boussinesqweg.

Deltares. (2019). *Technical user manual* (p. 1). Delft: Deltares, Boussinesqweg.

Hardy, R., Bates, P., & Anderson, M. (1999). The importance of spatial resolution in hydraulic models for floodplain environments. *Journal of Hydrology*, *216*(1), 124–136. https://doi.org/10.1016/S0022-1694(99)00002-5

Harlow, F. H., & Welch, J. E. (1965). Numerical calculation of time-dependent viscous incompressible flow of fluid with free surface. *The Physics of Fluids*, *8*(12), 2182–2189. https://doi.org/10.1063/1.1761178

Hoefsloot, F., & Van Doornik, W. (2020). *Dataprotocol Baseline 6.1.2*. Rijkswaterstaat WVL and Deltares. https://iplo.nl/thema/water/applicaties-modellen/watermanagementmodellen/baseline/

Huthoff, F., Ouwerkerk, S., Daggenvoorde, R., Snoek, Y., & Voortman, B. (2020). *Irm quickscan afvoercapaciteit*. Lelystad: Tech. rep., HKV lijn in water.

Ji, X., & Zhang, W. (2019). Tidal influence on the discharge distribution over the pearl river delta, China. *Regional Studies in Marine Science*, *31*, 100791. https://doi.org/10.1016/j.rsma.2019.100791

Kernkamp, H., Dam, A., Stelling, G., & Goede, E. (2011). Efficient scheme for the shallow water equations on unstructured grids with application to the continental shelf. *Ocean Dynamics*, *61*, 1175–1188. https://doi.org/10.1007/s10236-011-0423-6

Kleptsova, O., Pietrzak, J., & Stelling, G. (2009). On the accurate and stable reconstruction of tangential velocities in c-grid ocean models. *Ocean Modelling*, *28*(1), 118–126, the Sixth International Workshop on Unstructured Mesh Numerical Modelling of Coastal, Shelf and Ocean Flows. https://doi.org/10.1016/j.ocemod.2008.12.007

Lai, Y. (2010). Two-dimensional depth-averaged flow modeling with an unstructured hybrid mesh. *Journal of Hydraulic Engineering*, *136*(1), 12–23. https://doi.org/10.1061/(ASCE)HY.1943-7900.0000134

Langbein, W. B., & Leopold, L. B. (1966). *River meanders and the theory of minimum variance* (pp. 238–263). UK, London, chap 8: Palgrave Macmillan. https://doi.org/10.1007/978-1-349-15382-4-9

Meier, H., Alves, J., & Mori, M. (1999). Comparison between staggered and collocated grids in the finite-volume method performance for single and multi-phase flows. *Computers & Chemical Engineering*, *23*(3), 247–262. https://doi.org/10.1016/S0098-1354(98)00270-1

Minns, T., Spruyt, A., & Kerkhoven, D. (2019). *Specificaties zesde-generatie modellen met d-hydro* (p. 1). Tech. rep., Deltares, Boussinesqweg. https://publications.deltares.nl/11203714_013_0001.pdf

Mohamad, I. N., Lee, W. K., & May, R. (2016). Chapter 2. In *Idealized River meander using improved sine-generated curve method* In: Yusoff, M., Hamid, N., Arshad, M., Arshad, A., Ridzuan, A., & Awang, H. (Eds.), InCIEC 2015. Singapore: Springer. (pp. 125–135). https://doi.org/10.1007/978-981-10-0155-0-13

Mungkasi, S., Magdalena, I., Pudjaprasetya, S., Wiryanto, L., & Roberts, S. (2018). A staggered method for the shallow water equations involving varying channel width and topography. *International Journal for Multiscale Computational Engineering*, *16*, 231–244. https://doi.org/10.1615/IntJMultCompEng.2018027042

Parsapour-Moghaddam, P., Rennie, C., & Slaney, J. (2018). Hydrodynamic simulation of an irregularly meandering gravel-bed river: Comparison of mike 21 fm and delft3d flow models. In *River Flow 2018 - Ninth International Conference on Fluvial Hydraulics* (Vol. 40, 02004). River Flow 2018 - Ninth International Conference on Fluvial Hydraulics, Lyon-Villeurbanne. https://doi.org/10.1051/e3sconf/20184002004

Stelling, G. (1983). On the construction of computational methods for shallow water fow problems. *PhD thesis, Technical University of Delft*. http://resolver.tudelft.nl/uuid:d3b818cb-9f91-4369-a03e-d90c8c175a96

Tezdogan, T., Incecik, A., & Turan, O. (2016). A numerical investigation of the squat and resistance of ships advancing through a canal using cfd. *Journal of Marine Science and Technology*, *21*, 86–101. https://doi.org/10.1007/s00773-015-0334-1

Theodoropoulos, C., Stamou, A., Vardakas, L., Papadaki, C., Dimitriou, E., Skoulikidis, N., & Kalogianni, E. (2020). River restoration is prone to failure unless pre-optimized within a mechanistic ecological framework | insights from a model-based case study. *Water Research*, *173*, 115550. https://doi.org/10.1016/j.watres.2020.115550

Tu, J., Yeoh, G. H., & Liu, C. (2013). Chapter 5 - cfd solution analysis—Essentials. In J. Tu, G. H. Yeoh, & C. Liu (Eds.), *Computational fluid dynamics* (Second ed., pp. 177–217). Butterworth-Heinemann. https://doi.org/10.1016/B978-0-08-098243-4.00005-6

How to cite this article: Bilgili, E., Bomers, A., van Lente, G.-W., Huthoff, F., & Hulscher, S. J. M. H. (2023). The effect of a local mesh refinement on hydraulic modelling of river meanders. *River Research and Applications*, 1–15. https://doi.org/10.1002/rra.4110